

# Fast Dynamic 3D Object Generation from a Single-view Video

Zijie Pan<sup>1</sup>, Zeyu Yang<sup>1</sup>, Xiatian Zhu<sup>2</sup>, and Li Zhang<sup>1\*</sup>

<sup>1</sup> Fudan University

<sup>2</sup> University of Surrey

<https://fudan-zvg.github.io/Efficient4D>

**Abstract.** Generating dynamic 3D object from a single-view video is challenging due to the lack of 4D labeled data. Extending image-to-3D pipelines by transferring off-the-shelf image generation models such as score distillation sampling, existing methods tend to be slow and expensive to scale due to the need for back-propagating the information-limited supervision signals through a large pretrained model. To address this, we propose an efficient video-to-4D object generation framework called **Efficient4D**. It generates high-quality spacetime-consistent images under different camera views, and then uses them as labeled data to directly train a novel 4D Gaussian splatting model with explicit point cloud geometry, enabling real-time rendering under continuous camera trajectories. Extensive experiments on synthetic and real videos show that Efficient4D offers a remarkable 20-fold increase in speed when compared to prior art alternatives while preserving the quality of novel view synthesis. For example, Efficient4D takes only 6 mins to model a dynamic object, *vs* 120 mins by Consistent4D.

**Keywords:** 4D Generation · Gaussian Splatting · Video · Efficiency

## 1 Introduction

Humans possess a remarkable capacity to comprehensively comprehend the spatial and temporal characteristics of a dynamic object in a brief video, even with a limited perspective, enabling them to predict its appearance in unseen viewpoints over time. Despite the significant advancement of 3D object generation, existing works [4, 18, 29, 43] mostly consider static scenes or objects. With the availability of large-scale 3D datasets [5, 6], training generalizable models capable of directly generating multi-view images becomes possible [21–23]. These generated images can be turned into a 3D object through reconstruction techniques [26, 42]. By further augmenting these generated static objects with predefined animations [1], dynamic 3D content can be generated. However, this approach is still limited due to the need for fine-grained meshes as well as rigid restrictions.

---

\* Li Zhang (lizhangfd@fudan.edu.cn) is the corresponding author with School of Data Science, Fudan University.

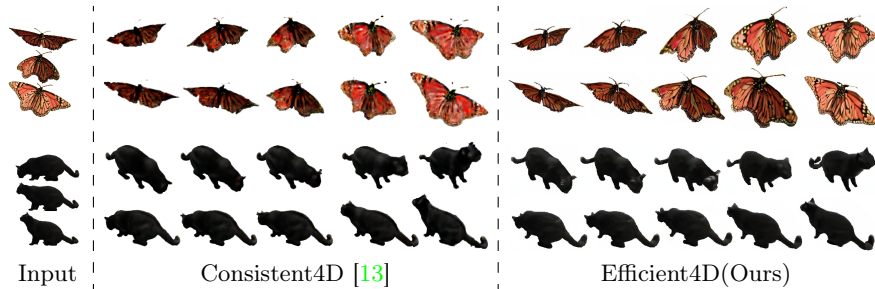


**Fig. 1:** Examples of video-to-4D generation. **Input:** A brief video of a dynamic object, as represented by 3 frames per case; **Output:** Generated novel views at different timestamps.

Directly generating 4D object/scene content from text description has been recently attempted [38]. To bypass the need of exhaustively labeled training data pairs in form of (text, 4D), it trains a Neural Radiance Fields (NeRF)-like representation [26] via score distillation sampling [29] and separates the modeling of static scene and its dynamics. Not only is this method computationally inefficient caused by heavy supervision back-propagation through a large pre-trained model, but also its textual condition is highly ambiguous in expressing the intended visual content. In quest of the aforementioned human’s capability, a recent work [13] proposed to generate dynamic 3D object images from a single-view video (statically captured monocular video from a fixed view), namely as *video-to-4D* object generation. However, similar as [38] this method is also slow to train (e.g., 150 minutes to model a single dynamic object) in addition to complex design, hence unscalable and expensive in practice.

To address identified limitations, we formulate an efficient video-to-4D two staged object generation method called *Efficient4D*. In the first stage, we generate spacetime-consistent images across different camera views as synthetic training data. This is realized by imposing temporal smoothing into a multi-view image generator (e.g., SyncDreamer [22]) in tandem with frame interpolation. In the second stage, we use these training data to optimize a novel 4D Gaussian splatting model. This is an extension of the 3D Gaussian splatting [15], originally designed for static 3D scene representation, with the temporal dimension introduced additionally. Using Gaussian representation brings about further computational efficiency gain along with the explicit geometry property, when compared with NeRF based designs (Fig. 1). To tackle the challenging discontinuity between generated frames, we design an inconsistency-aware loss function.

Our **contributions** are summarized as follows: **(i)** We consider for the first time the efficiency challenge with the under-studied video-to-4D object generation problem. **(ii)** We propose an efficient video-to-4D object generation pipeline, *Efficient4D*, characterized by directly generating high-quality training data without the need for heavy supervision back-propagation through a large pretrained model as suffered by most 3D/4D object generation approaches. **(iii)** Instead

of using NeRF as the 3D representation model, we introduce a novel 4D Gaussian splatting model with the real-time rendering advantage. **(iv)** Extensive experiments on both synthetic and real videos validate the significant efficiency advantage (e.g.,  $20\times$  speedup) of our Efficient4D over the prior art, whilst maintaining the quality of novel view synthesis. Also, our method can work well under the more challenging few-shot setting where only a handful of key frames are available for training, further extending the application scope.

## 2 Related work

**3D generation** 3D generation takes two main settings: text-to-3D and image-to-3D. The pioneering work, DreamFusion [29], introduces the score distillation sampling (SDS) loss for optimizing 3D shapes with diffusion models. SDS’s generality has prompted numerous subsequent efforts in both text-to-3D tasks [4, 11, 16, 18, 25, 34, 36, 41, 43, 47, 52] and image-to-3D tasks [24, 31, 40, 48] across various dimensions. However, SDS-based approaches often suffer from extended optimization times. Conversely, some efficient methods [14, 20–22, 27] have emerged. Notably, Point-E [27] and Shap-E [14] train models to directly generate 3D point clouds or meshes. Zero123 [21] focuses on generating a 2D image from an unseen view based on a single image, convertible to a 3D shape through SDS or [20]. Importantly, SyncDreamer [22] produces multi-view consistent images, offering inspiration for reconstructing 3D objects.

**4D representation** Efforts to synthesize videos with free-viewpoint control in dynamic scenes have a well-documented history [53]. For example, pre-NeRF [26] approaches challenges in reconstructing intricate scene details. Recent advancements in 4D representations, particularly those based on neural rendering, include D-NeRF [30], DeVRF [19] and HyperNeRF [28], which decouple geometry and motion, utilizing a canonical space and a learned deformation field. DynI-BaR [17] deploys an image-based rendering paradigm for representing long videos with complex camera and object motions. Another group of methods [3, 8, 35] adopt tensor decomposition of 4D volumes to represent dynamic 3D scenes.

Recently, Gaussian Splatting [15] has received widespread attention for its real-time high-fidelity rendering, especially its explicit point-based representation which holds great potential in modeling dynamic scenes. Consequently, a significant amount of work has been proposed to explore its extension to dynamic scene modeling. Among them, Deformable 3D Gaussians [49] and 4DGaussian [46] integrated the deformation field with 3D Gaussian Splatting for the joint learning of the scene’s geometry and dynamics. SC-GS [10] represents the motion with a set of sparse control points to achieve reconstruction and motion editing. Unlike the previous radiance field-based representations often involving complex training schedules or suffering from slow convergence, these methods can be optimized efficiently, achieving real-time rendering while surpassing the past methods in terms of quality.

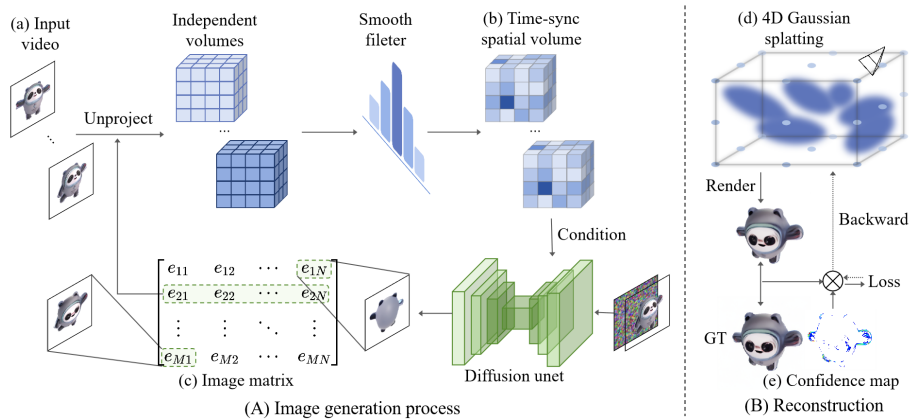


**Fig. 2: Overview of our Efficient4D approach.** Given as the input a brief video depicting a dynamic object from a single perspectives, our model aims to generate this object with geometrical and temporal consistency under any specific view and time. Efficient4D comprises two components: **(A)** Image sequence synthesis across views and timesteps, resulting in (c) an *image matrix* where each row consists of multi-view geometrically consistent images and each column consists of view-specific temporally consistent images. **(B)** A novel 4D Gaussian representation model (d) that represents the scene with a number of Gaussian points. It can be trained efficiently and robustly under the confidence-aware (e) supervision on the generated image matrix.

Our work is perpendicular to all the above works, where any of them can be deployed in our reconstruction phase. But considering both optimization efficiency and expressive capability, we propose to represent dynamic 3D assets by a set of native 4D scene primitives.

**4D generation** There are a few recent works dedicated for more challenging 4D object generation. For instance, MAV3D [38] deals with a text-to-4D problem by training Hexplane [3] with a video diffusion model and SDS loss. Instead of text input, Consistent4D [13] conditions the generation of 4D object over time on a monocular video with richer and more specific information. However, it is computationally inefficient due to inheriting the previous SDS loss, along with complex pipeline design. To overcome this limitation, we present a novel two-staged pipeline in a generation-and-reconstruction strategy, drastically boosting the training speed by  $20\times$  whilst maintaining the quality of novel view synthesis.

### 3 Method

Our Efficient4D addresses the challenge of efficiently generating dynamic objects under novel views from a single-view video. As illustrated in Fig. 2, it comprises two key components:



- An image synthesis pipeline (Sec. 3.1) generates images across views and timestamps, ensuring sufficient geometry and temporal consistency.
- A novel 4D Gaussian representation model (Sec. 3.2) efficiently utilizes the synthetic images for accurate dynamic object reconstruction and novel view synthesis.

### 3.1 Image synthesis across views and timestamps

Due to the difficulty of obtaining calibrated 4D scans, our approach involves the direct generation of high-quality consistent 4D data from a single-view video which is much easier to capture (Fig. 2(A)). Specifically, we seek to produce a  $M \times N$  **image matrix**  $\mathcal{D} = \{e_{ij}\}_{i,j=1}^{M,N}$  representing 2D images with geometrical and temporal consistency. Here,  $M$  denotes timestamps, and  $N$  represents views, with each matrix element corresponding to an image (Fig. 2(c)). This approach combines conventional video (capturing time variation, represented by a single column in the image matrix) and 3D (capturing view variation, represented by a single row in the image matrix) generation [22, 37], offering comprehensive information for modeling a dynamic object.

To initiate the image matrix  $\mathcal{D}$ , we set the first view (i.e., the first column) with  $K$  frames from the input video (Fig. 2(a)) and proceed to generate the remaining views. Our task involves generating multi-view consistent images from a single image for each row. Existing image-to-3D methods, such as SyncDreamer [22], can be leveraged for this purpose. However, these methods often struggle with temporal inconsistency within a specific view (i.e., continuity in the column direction) due to the independent synthesis of multi-frame images. To address this issue, we propose an enhanced version of SyncDreamer with improved temporal continuity, referred to as **SyncDreamer-T**.

Specifically, SyncDreamer generates  $N$  multi-view images  $\{\mathbf{x}_0^{(1)}, \dots, \mathbf{x}_0^{(N)}\}$  of a static object using a synchronized  $N$ -view noise predictor  $\{\epsilon_\theta^{(n)} | n = 1, \dots, N\}$  that predicts synchronized noise for noisy multi-view images  $\mathbf{x}_t^{1:N}$ . The noise predictor is conditioned on information correlated with all views. Cross-view conditioning is achieved through a spatial feature volume  $\mathcal{V} \in \mathbb{R}^{F \times V \times V \times V}$  unprojected by  $\mathbf{x}_t^{1:N}$  to inject 3D-aware features into the shared noise predictor, ensuring geometrical consistency across views for static moments.

To impose temporal consistency, the information from  $\mathcal{V}$  at different timestamps is aggregated using a time-synchronous spatial volume we design here (Fig. 2(b)). A smoothing filter layer is introduced into the spatial volumes of different frames/timestamps, incorporating a weight vector  $\mathbf{w} = (w_{-k}, \dots, w_0, \dots, w_k)$ . At each denoising step, time-synchronized spatial volumes  $\tilde{\mathcal{V}}_i$  for each input frame  $i \in \{1, 2, \dots, M\}$  are constructed as:

$$\tilde{\mathcal{V}}_i = \sum_{j=-k}^k w_{i+j} \mathcal{V}_{i+j}. \quad (1)$$

This synchronization ensures consistent features across  $k$  past and  $k$  future frames during the denoising process, enhancing temporal consistency. With this

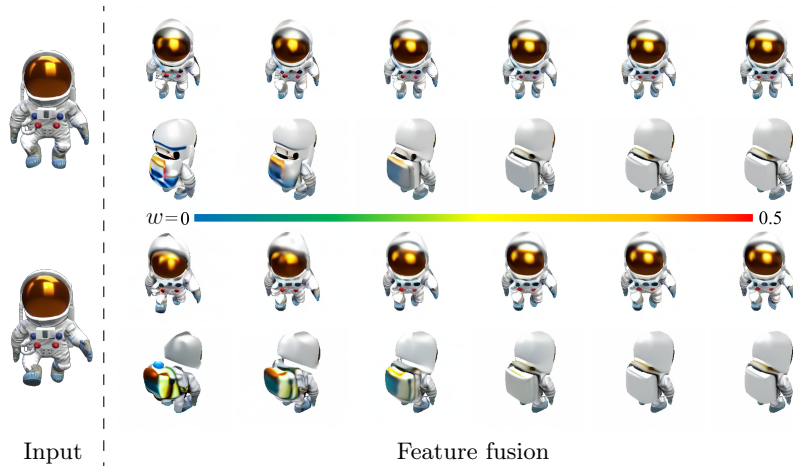


**Fig. 3: Example analysis on temporal synchronization.** In this illustration, we manipulate the fusion ratio ( $w$ ) across a range from 0 to 0.5 for the spatial feature volumes of two input frames. The results indicate that a moderate ratio can achieve superior outcomes by balancing both temporal consistency and motion independence.

time-synchronized spatial volumes, the proposed *SyncDreamer-T* is entirely *training-free* established on the pretrained SyncDreamer.

To further improve temporal resolution, video frame interpolation (e.g., RIFE [12]) is applied after generating the image matrix  $\mathcal{D}$  as described above. The midpoint interpolation is applied twice recursively, giving three additional frames between each pair of consecutive frames. This results in a total of  $M = 4K - 3$  images in a column of  $\mathcal{D}$ .

**Analysis on temporal synchronization** For a clearer insight into our temporal synchronization design, we undertake a simplified experiment involving two input frames, each with its feature volumes labeled as  $\mathcal{V}_1$  and  $\mathcal{V}_2$ . The fusion process is carried out by combining them as follows:

$$\tilde{\mathcal{V}}_i = (1 - w)\mathcal{V}_i + w\mathcal{V}_{3-i}, \quad (2)$$

where  $i \in \{1, 2\}$  and  $w$  denotes the fusion ratio, we systematically vary the ratio  $w$  from 0 to 0.5, resulting in distinct columns of “Feature fusion” as illustrated in Fig. 3. For  $w = 0$ , the original generation process is represented, where the spatial volumes of the two frames are independent, leading to temporal inconsistency. As  $w$  approaches 0.5, we observe a gradual convergence of the generated astronauts conditioned on different input images, achieving similarity in both texture and geometry. This suggests that smoothing at the feature level is effective in aligning frames over time.

However, a challenge arises as the fused features may induce similar motion. While the bottom-left astronaut is stepping forward, the one at the bottom-right

column does not exhibit forward motion like the top astronaut. Thus, a trade-off is necessary between achieving temporal consistency and preserving motion independence. In practical terms, it is recommended to set the ratio between 0.25 and 0.4, striking a balance that ensures temporal texture consistency at a moderate cost of entangled geometry. Note that the results in Fig. 3 are not sensitive to the choice in this range.

### 3.2 4D generation through reconstruction

Aiming for 3D dynamic object modeling, discrete images not suffice. Our next goal is to model a truly 4D content from the image matrix  $\mathcal{D}$ . For efficient modeling, we formulate a novel 4D Gaussian representation model (Fig. 2(B)), departing from previous slow-to-train 4D reconstruction models [8].

**4D Gaussian representation model** Our model builds upon the 3D Gaussian splatting technique introduced in [15], originally designed for static scene representation. We extend it to address the complexities of dynamic scenes, enabling the real-time synthesis of high-fidelity views in 4D space. The model represents each Gaussian defined as:

$$G(\mathbf{p}|\mu, \Sigma) = e^{-\frac{1}{2}(\mathbf{p}-\mu)^\top \Sigma^{-1}(\mathbf{p}-\mu)}, \quad (3)$$

where  $\mu \in \mathbb{R}^4$  is the mean vector, and  $\Sigma \in \mathbb{R}^{4 \times 4}$  is the anisotropic covariance matrix. The input  $\mathbf{p} = (\mathbf{x}, t) \in \mathbb{R}^4$  represents a spacetime position with a spatial coordinate  $\mathbf{x}$  and time  $t$ . The covariance matrix  $\Sigma$  decomposes into a diagonal scaling matrix  $S \in \mathbb{R}^{4 \times 4}$  and a rotation matrix  $R \in \mathbb{R}^{4 \times 4}$  through  $\Sigma = RSS^\top R^\top$ . The 4D rotation  $R$  is represented by a pair of iso-rotations, each characterized by a quaternion.

In contrast to the 3D counterpart, our formulation incorporates the time dimension, allowing coherent modeling of dynamics in both space and time.

**Rendering** For rendering, each Gaussian includes opacity  $\alpha$  and view-dependent color  $\mathbf{c}$  represented by spherical harmonics (SH). Given an arbitrary view  $\mathcal{I}$  defined by intrinsic and extrinsic parameters, we render the pixel at position  $(u, v)$  with timestamp  $t$  by blending visible Gaussians:

$$\mathcal{I}(u, v, t) = \sum_i f_i(u, v, t) \alpha_i \mathbf{c}_i(d) T_i \quad (4)$$

$$\text{with } T_i = \prod_{j=1}^{i-1} (1 - f_j(u, v, t) \alpha_j). \quad (5)$$

Here,  $i$  indexes the visible Gaussians sorted by depth,  $d$  refers to the direction of the pixel under the view  $\mathcal{I}$ , and  $f_i(u, v, t)$  denotes the influence of a Gaussian on this position. To obtain the influence, unlike 3D Gaussian Splatting [15] which

directly projects 3D Gaussians to image space, we need condition 4D Gaussians on time and then project them. More specifically,  $f(u, v, t)$  is expressed by:

$$f(u, v, t) = G_t(t|\mu_t, \Sigma_t)G_{P(\mathbf{x})|t}(u, v|P(\mu_{\mathbf{x}|t}), P(\Sigma_{\mathbf{x}|t})), \quad (6)$$

where  $G_t$  is the marginal distribution of the 4D Gaussian in time, and  $G_{P(\mathbf{x})|t}$  is the projected version of the conditional 3D Gaussian with

$$\mu_{\mathbf{x}|t} = \mu_{\mathbf{x}} + \Sigma_{\mathbf{x},t}\Sigma_t^{-1}(t - \mu_t), \quad (7)$$

$$\Sigma_{\mathbf{x}|t} = \Sigma_{\mathbf{x}} - \Sigma_{\mathbf{x},t}\Sigma_t^{-1}\Sigma_{t,\mathbf{x}}. \quad (8)$$

The projection operation  $P$  [15, 54] projects the world point  $\mu_{\mathbf{x}|t}$  to image space and transforms the covariance by  $P(\Sigma_{\mathbf{x}|t}) = JW\Sigma_{\mathbf{x}|t}W^\top J^\top$  where  $W$  is the extrinsic matrix of  $\mathcal{T}$  and  $J$  is the Jacobian of the affine approximation of the projective transformation.

**Optimization** In training, optimization is performed on the mean ( $\mu$ ), covariance ( $\Sigma$ ), opacity ( $\alpha$ ), and spherical harmonic (SH) coefficients, as well as density control including densification and pruning for each Gaussian. The original objective function, as presented in [15], assumes clean training data, which may not less valid for synthetic data with inherent imperfections. To address this, we introduce a confidence-aware objective loss formulation defined as:

$$\mathcal{L} = \lambda_{\text{rgb}}\mathcal{C}_{\text{rgb}}\mathcal{L}_{\text{rgb}} + \lambda_{\text{ssim}}\mathcal{C}_{\text{ssim}}\mathcal{L}_{\text{ssim}}, \quad (9)$$

where  $\mathcal{L}_{\text{rgb}}$  is the  $L_1$  loss in RGB space,  $\mathcal{L}_{\text{ssim}}$  is the SSIM loss [44],  $\lambda_{\text{rgb}/\text{ssim}}$  is the respective weight hyper-parameter, and  $\mathcal{C}_{\text{rgb}/\text{ssim}}$  is the confidence score of a generated image  $\mathbf{I}$  calculated as

$$\mathcal{C}_{\text{rgb}} = 1 - |\mathbf{I} - \hat{\mathbf{I}}|, \quad \mathcal{C}_{\text{ssim}} = \text{SSIM}(\mathbf{I}, \hat{\mathbf{I}}) \quad (10)$$

where  $\hat{\mathbf{I}}$  is the unwarped image from adjacent frames estimated by optical flow. In such way, the confidence  $\mathcal{C}_{\text{rgb}/\text{ssim}}$  function as an adaptive role in controlling the loss and gradient by assigning lower weights to inconsistent regions.

## 4 Experiments

### 4.1 Implementation details

**Competitors** Video-to-4D is a relatively unexplored area, with only one existing method, Consistent4D [13]. In comparison, we obtained the results of Consistent4D by running its released code. We also compare SyncDreamer [22] partially by replacing SyncDreamer-T in Sec. 4.5.



**Fig. 4: Qualitative evaluation** of Consistent4D (C4D) [13] and our method against ground truth (GT) on synthetic data.

**Evaluation videos** To showcase the versatility of our proposed method, we conducted extensive experiments using a diverse set of data sources. Specifically, we focused on 36 sequences: 32 sequences released by [13] and 4 sequences processed by ourselves. Among the released data, seven sequences are synthetic data where ground truth are provided. Our four sequences are used for sparse input evaluation in Sec. 4.4, which only contain two frames for each sequence. Three of them, named *dragon*, *guard*, and *yoxi*, are rendered from 3D animated models obtained from Sketchfab [2]. The other one named *yellow face* was collected from the internet. Each sequence consists of monocular videos captured by a stationary camera, with duration ranging from approximately 1s to 3s.

**Evaluation metrics** As 4D generation research is still at early stage, there is no well established metric yet. However, we adopt multiple metrics by referring related works for comprehensive evaluation. For evaluating on synthetic data, we use LPIPS score [51] and CLIP similarity [32] between rendered images and ground truth following [13]. For the cases without ground truth, we also use CLIP-similarity between generated images and input frames as [33, 39] to measure image quality. For temporal smoothness, following [7, 9, 50] we use CLIP-T to measure the similarity between adjacent frames of a generated video from different views, including front (CLIP-T-f), side (CLIP-T-s) and back (CLIP-T-b) views. To evaluate a 4D object completely for different methods, we obtain the generated images by rendering 320 images uniformly distributed in space and time, covering 16 viewpoints and 20 timestamps.

**Implementation** For SyncDreamer-T, we typically set the weight as  $\mathbf{w} = (0.1, 0.1, 0.6, 0.1, 0.1)$  in time-synchronous spatial volume. The improved sampling strategy [45] can be seamlessly integrated into SyncDreamer-T. In the reconstruction stage, we implement a modified CUDA rasterizer tailored to 4D



**Fig. 5: Qualitative comparisons.** We show four images per method, captured from two viewpoints at two timestamps. Our geometry is the points at 3D mean of Gaussians.

Gaussian. Gaussians are initialized randomly within the space  $[-0.6, 0.6]^3$  with identity rotations and a initial number of 20,000. Training of 4D Gaussian Splatting is carried out using the Adam optimizer for 20,000 iterations with a batch size of 2. Gaussians are densified every 200 iterations, with densification halted at the 10,000th iteration. All other hyperparameters remain consistent with those in [15]. For speed efficiency, our proposed method only costs about 2 minutes for image generation and 4 minutes for reconstruction on one A6000 GPU.

## 4.2 Qualitative evaluation

We first present the results on synthetic data in Fig. 4 with ground truth shown. Our visual results exhibit superior accuracy in both texture and geometry when compared to the ground truth. For other data without ground truth, we present qualitative comparisons in Fig. 5. In geometry rendering, we extract points at the mean of Gaussians. We also eliminate white background points and transparent points with low opacity. When assessing texture quality, it is important to note that both methods fall under the category of lifting 2D to 4D. However,

**Table 1: Quantitative comparisons.** The frame per second (FPS) is evaluated using a  $256 \times 256$  resolution rendering. <sup>†</sup>: Measured using code released by Consistent4D [13] with one A6000 GPU.

	Consistent4D [13]	Efficient4D(Ours)
<i>- Comparison with ground truth on synthetic data</i>		
CLIP $\uparrow$	0.87	<b>0.92</b>
LPIPS $\downarrow$	0.16	<b>0.14</b>
<i>- Comparison on all cases</i>		
CLIP $\uparrow$	0.8471	<b>0.8721</b>
CLIP-T-f $\uparrow$	0.9692	<b>0.9702</b>
CLIP-T-s $\uparrow$	0.9658	<b>0.9726</b>
CLIP-T-b $\uparrow$	0.9697	<b>0.9707</b>
Generation time $\downarrow$	120 mins <sup>†</sup>	<b>6 mins</b>
FPS $\uparrow$	$\sim 20^{\dagger}$	<b><math>\sim 1000</math></b>
Explicit geometry	<b><math>\times</math></b>	<b><math>\checkmark</math></b>

Consistent4D produces watercolor-like images with low fidelity, which can be attributed to conflicts from multiple supervisory signals during prolonged optimization. In contrast, our method excels in directly generating high-quality 2D images. Subsequently, our method’s reconstruction stage yields explicit point clouds and exhibits less degradation in rendering quality compared to the SDS-based Consistent4D. Overall, our method consistently outperforms Consistent4D in most cases.

### 4.3 Quantitative evaluation

In Tab. 1, we compare Consistent4D and our method quantitatively. The metrics and data used are described in Sec. 4.1.

We draw several observations: **(1)** For synthetic data, our generation results produce better CLIP and LPIPS scores. **(2)** Our method achieves superior image quality and temporal smoothness on all cases. **(3)** Our method significantly accelerates the generation process, achieving over  $20\times$  speed improvement. **(4)** Our efficient 4D Gaussian representation and splatting based rendering enable real-time rendering and provide explicit point cloud geometry.

More specifically, the speed improvement is attributed to **(1)** our SDS-free design, converging optimization faster, and **(2)** each iteration in our method requiring much less time compared to Consistent4D. This time efficiency is further enhanced by avoiding recurrent evaluation in the diffusion model and prolonged forward rendering of the inefficient 4D representation as needed in the competitor at every iteration.



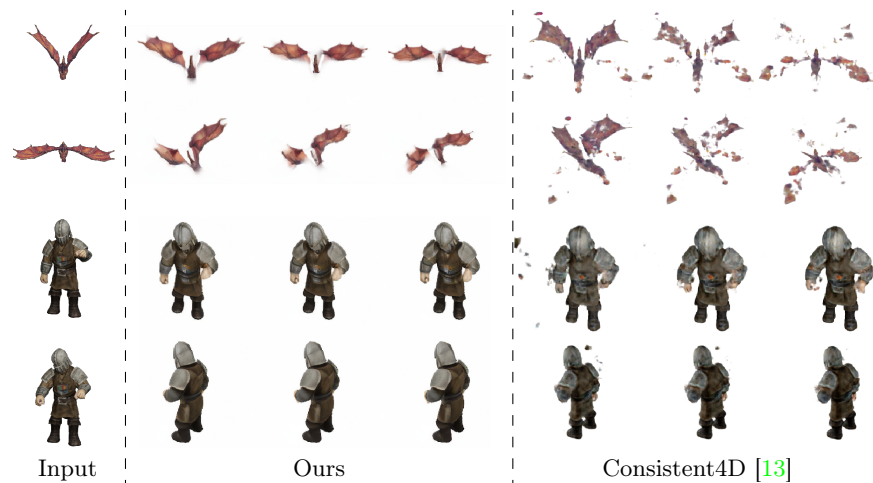


**Fig. 6:** Given only two input frames, our method is able to generate smooth dynamics. For each case, we show three internal images from two novel views.

**Table 2: Quantitative ablation study** on all our modules measured on 4 sequences: alpaca, astronaut, rabbit and spiderman.

Method	CLIP $\uparrow$	CLIP-T-f $\uparrow$	CLIP-T-s $\uparrow$	CLIP-T-b $\uparrow$
Single-view	0.6684	-	-	-
No time-sync	0.8270	0.9258	0.9197	0.8819
No interp	0.8595	0.9409	0.9443	0.9336
No conf	0.8611	0.9658	0.9592	0.9611
Full setting	<b>0.8702</b>	<b>0.9689</b>	<b>0.9673</b>	<b>0.9684</b>

#### 4.4 Sparse input evaluation

We assessed our method’s performance in an extremely sparse input scenario, comprising only two discrete frames. In such cases, we set  $w = 0.25$  in Eq. (2). As illustrated in Fig. 6, our approach successfully generates images featuring smooth motion and high spatiotemporal consistency. In contrast, Consistent4D fails to operate effectively under such conditions.

Consider a scenario where we seek 4D modeling for a static toy. While the toy can take different poses, it lacks autonomous movement, posing a challenge for continuous video capturing. In these instances, our method demonstrates effectiveness by requiring only a few key frames to produce dynamic content, thereby expanding the potential applications of the video-to-4D task.

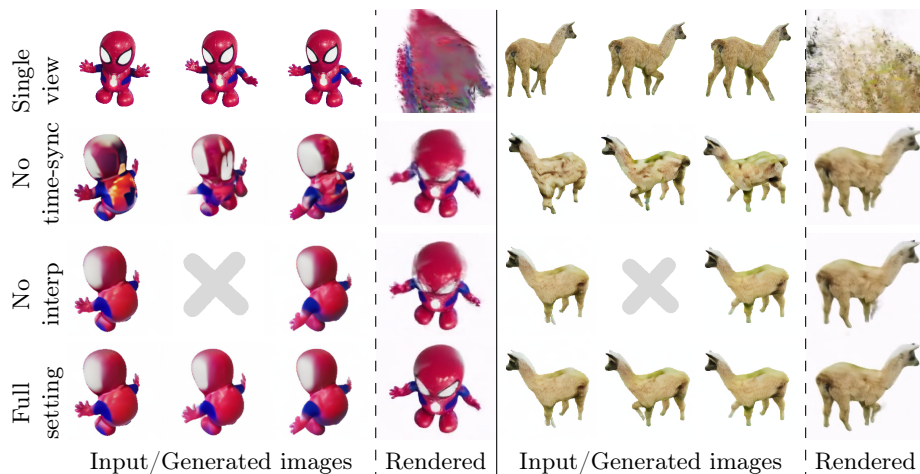


**Fig. 7: Ablation study** on image generation, time-synchronous spatial volumes and frame interpolation. The images follow a chronological order from left to right.

#### 4.5 Ablation studies

We performed ablation studies to assess the influence of different components in our approach. We compared our full method against five baseline settings: **(1)** Only input video are used for reconstruction; **(2)** Time-synchronous spatial volume is excluded; **(3)** Frame interpolation is excluded; **(4)** Confidence maps are excluded; **(5)** 4D Gaussian splatting is replaced with K-Plane [8]. Note setting **(2)** is equivalent to the case where SyncDreamer-T is replaced with original SyncDreamer. The results corresponding to these settings can be found in Fig. 7 and Fig. 8. Table 2 also gives quantitative evaluations.

**Importance of synthetic data.** We compare our generated image matrix with utilizing only input video using the same proposed 4D Gaussian representation model. As shown in the first row of Fig. 7, when only relying on a single-view video, the model cannot produce any meaningful results for novel views. This indicates the importance of constructing proper training data.

**Effect of time-synchronous spatial volume.** We assess the impact of the time-synchronous spatial volume concept introduced in SyncDreamer, as depicted in the contrast of the second and last rows in Fig. 7 and Tab. 2. Without time-synchronous spatial volume, the back aspects of the toy Spiderman exhibit inconsistencies, leading to distorted geometry. In contrast, the proposed time-synchronous spatial volume enhances both spatial and temporal consistency while preventing geometry collapse, resulting in more visually appealing image generation and higher CLIP-T scores.

**Effect of frame interpolation.** As illustrated in the contrast between the third and last rows in Fig. 7 and Tab. 2, frame interpolation is effective in

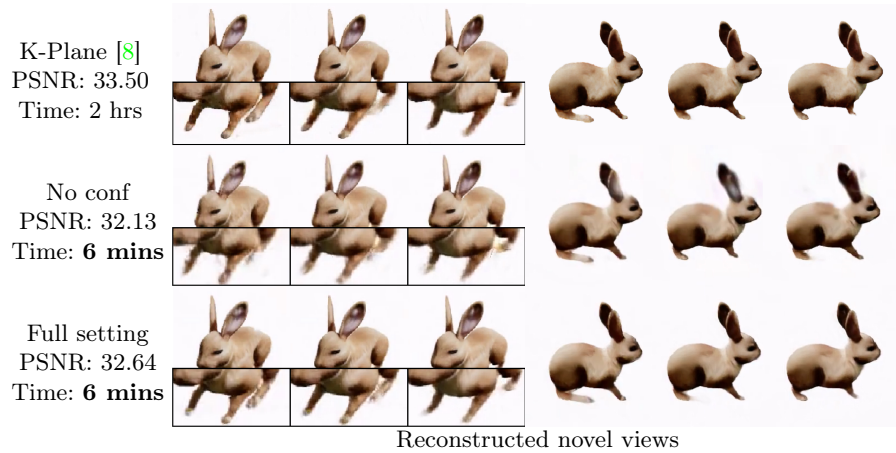


**Fig. 8: Ablation study** on 4D scene representation and confidence maps. The images follow a chronological order from left to right.

mitigating the blurring observed in the rendered image from novel views, thus delivering higher CLIP-T scores. This is attributed to the low frame rates of the image matrix, which results in noticeable discontinuities.

**Effect of confidence-aware in objective.** The integration of a confidence-aware loss in our design serves as a strategy to mitigate training data noise. This is evident in the contrast between the “No conf” and “Full setting” results in Fig. 8 and Tab. 2. The inclusion of confidence maps effectively reduces blurry rendering caused by inter-frame inconsistency, resulting in a significant overall improvement in quality and temporal smoothness.

**Integrating existing 4D representation model.** Our synthetic training data is versatile and supports the optimization of 4D representation models, such as K-Plane [8]. In the comparison shown in Fig. 8, our 4D Gaussian splatting and K-Plane exhibit comparable proficiency in reconstructing dynamic scenes. Notably, our method surpasses K-Plane in speed, achieving a  $20\times$  improvement. Additionally, as emphasized in Sec. 4.3, our model enables real-time rendering with explicit point cloud geometry.

## 5 Conclusion

This study introduces a new framework, Efficient4D, designed for generating efficiently dynamic 4D objects seamlessly from monocular videos captured by a stationary camera. The Efficient4D consists of two main stages: first, generating consistent multi-view videos with spatial and temporal coherence, and second, rapidly producing 4D object reconstructions using an innovative 4D Gaussian

splatting model. Our approach, utilizing SDS-Free design and efficient 4D representation, significantly accelerates the generation process, achieving over 20 times faster speeds compared to previous work, while still delivering superior reconstruction and novel view synthesis results. Moreover, our model is effective in extremely sparse input scenarios, requiring only two available images, thereby expanding its application scope.

**Limitations.** Our local smoothing approach in sliding window style with our image sequence generator poses challenges in handling long-duration videos. To address this issue, replacing the smoothing filtering layer with a learnable attention layer featuring global receptive fields is a viable solution, particularly when dealing with extensive 4D datasets. Additionally, handling long videos may necessitate significant GPU memory, which can be mitigated by employing multi-GPUs or CPUs, albeit with an increase in processing time.

## References

1. Maximo. <https://www.mixamo.com/> (2023) 1
2. Sketchfab. <https://sketchfab.com/> (2023) 9
3. Cao, A., Johnson, J.: Hexplane: A fast representation for dynamic scenes. In: ICCV (2023) 3, 4
4. Chen, R., Chen, Y., Jiao, N., Jia, K.: Fantasia3d: Disentangling geometry and appearance for high-quality text-to-3d content creation. In: ICCV (2023) 1, 3
5. Deitke, M., Liu, R., Wallingford, M., Ngo, H., Michel, O., Kusupati, A., Fan, A., Laforte, C., Voleti, V., Gadre, S.Y., et al.: Objaverse-xl: A universe of 10m+ 3d objects. In: NeurIPS (2023) 1
6. Deitke, M., Schwenk, D., Salvador, J., Weihs, L., Michel, O., Vanderbilt, E., Schmidt, L., Ehsani, K., Kembhavi, A., Farhadi, A.: Objaverse: A universe of annotated 3d objects. In: CVPR (2023) 1
7. Esser, P., Chiu, J., Atighehchian, P., Granskog, J., Germanidis, A.: Structure and content-guided video synthesis with diffusion models. In: ICCV (2023) 9
8. Fridovich-Keil, S., Meanti, G., Warburg, F.R., Recht, B., Kanazawa, A.: K-planes: Explicit radiance fields in space, time, and appearance. In: CVPR (2023) 3, 7, 13, 14
9. Geyer, M., Bar-Tal, O., Bagon, S., Dekel, T.: Tokenflow: Consistent diffusion features for consistent video editing. arXiv preprint (2023) 9
10. Huang, Y.H., Sun, Y.T., Yang, Z., Lyu, X., Cao, Y.P., Qi, X.: Sc-gs: Sparse-controlled gaussian splatting for editable dynamic scenes. In: CVPR (2024) 3
11. Huang, Y., Wang, J., Shi, Y., Qi, X., Zha, Z.J., Zhang, L.: Dreamtime: An improved optimization strategy for text-to-3d content creation. In: CVPR (2023) 3
12. Huang, Z., Zhang, T., Heng, W., Shi, B., Zhou, S.: Real-time intermediate flow estimation for video frame interpolation. In: ECCV (2022) 6
13. Jiang, Y., Zhang, L., Gao, J., Hu, W., Yao, Y.: Consistent4d: Consistent 360° dynamic object generation from monocular video. In: ICLR (2024) 2, 4, 8, 9, 10, 11, 12
14. Jun, H., Nichol, A.: Shap-e: Generating conditional 3d implicit functions. arXiv preprint (2023) 3

15. Kerbl, B., Kopanas, G., Leimkühler, T., Drettakis, G.: 3d gaussian splatting for real-time radiance field rendering. In: ACM TOG (2023) [2](#), [3](#), [7](#), [8](#), [10](#)
16. Li, Y., Dou, Y., Shi, Y., Lei, Y., Chen, X., Zhang, Y., Zhou, P., Ni, B.: Focal-dreamer: Text-driven 3d editing via focal-fusion assembly. In: PLMR (2023) [3](#)
17. Li, Z., Wang, Q., Cole, F., Tucker, R., Snavely, N.: Dynibar: Neural dynamic image-based rendering. In: CVPR (2023) [3](#)
18. Lin, C.H., Gao, J., Tang, L., Takikawa, T., Zeng, X., Huang, X., Kreis, K., Fidler, S., Liu, M.Y., Lin, T.Y.: Magic3d: High-resolution text-to-3d content creation. In: CVPR (2023) [1](#), [3](#)
19. Liu, J.W., Cao, Y.P., Mao, W., Zhang, W., Zhang, D.J., Keppo, J., Shan, Y., Qie, X., Shou, M.Z.: Devrf: Fast deformable voxel radiance fields for dynamic scenes. In: NeurIPS (2022) [3](#)
20. Liu, M., Xu, C., Jin, H., Chen, L., Xu, Z., Su, H., et al.: One-2-3-45: Any single image to 3d mesh in 45 seconds without per-shape optimization. arXiv preprint (2023) [3](#)
21. Liu, R., Wu, R., Van Hoorick, B., Tokmakov, P., Zakharov, S., Vondrick, C.: Zero-1-to-3: Zero-shot one image to 3d object. In: ICCV (2023) [1](#), [3](#)
22. Liu, Y., Lin, C., Zeng, Z., Long, X., Liu, L., Komura, T., Wang, W.: Syncdreamer: Learning to generate multiview-consistent images from a single-view image. In: ICLR (2024) [1](#), [2](#), [3](#), [5](#), [8](#)
23. Long, X., Guo, Y.C., Lin, C., Liu, Y., Dou, Z., Liu, L., Ma, Y., Zhang, S.H., Habermann, M., Theobalt, C., et al.: Wonder3d: Single image to 3d using cross-domain diffusion. arXiv preprint (2023) [1](#)
24. Melas-Kyriazi, L., Laina, I., Ruppel, C., Vedaldi, A.: Realfusion: 360deg reconstruction of any object from a single image. In: CVPR (2023) [3](#)
25. Metzger, G., Richardson, E., Patashnik, O., Giryes, R., Cohen-Or, D.: Latent-nerf for shape-guided generation of 3d shapes and textures. In: CVPR (2023) [3](#)
26. Mildenhall, B., Srinivasan, P.P., Tancik, M., Barron, J.T., Ramamoorthi, R., Ng, R.: Nerf: Representing scenes as neural radiance fields for view synthesis. Communications of the ACM (2021) [1](#), [2](#), [3](#)
27. Nichol, A., Jun, H., Dhariwal, P., Mishkin, P., Chen, M.: Point-e: A system for generating 3d point clouds from complex prompts. arXiv preprint (2022) [3](#)
28. Park, K., Sinha, U., Hedman, P., Barron, J.T., Bouaziz, S., Goldman, D.B., Martin-Brualla, R., Seitz, S.M.: Hypernerf: a higher-dimensional representation for topologically varying neural radiance fields. In: ACM TOG (2021) [3](#)
29. Poole, B., Jain, A., Barron, J.T., Mildenhall, B.: Dreamfusion: Text-to-3d using 2d diffusion. In: ICLR (2023) [1](#), [2](#), [3](#)
30. Pumarola, A., Corona, E., Pons-Moll, G., Moreno-Noguer, F.: D-nerf: Neural radiance fields for dynamic scenes. In: CVPR (2021) [3](#)
31. Qian, G., Mai, J., Hamdi, A., Ren, J., Siarohin, A., Li, B., Lee, H.Y., Skorokhodov, I., Wonka, P., Tulyakov, S., et al.: Magic123: One image to high-quality 3d object generation using both 2d and 3d diffusion priors. In: ICLR (2024) [3](#)
32. Radford, A., Kim, J.W., Hallacy, C., Ramesh, A., Goh, G., Agarwal, S., Sastry, G., Askell, A., Mishkin, P., Clark, J., et al.: Learning transferable visual models from natural language supervision. In: ICML (2021) [9](#)
33. Ren, J., Pan, L., Tang, J., Zhang, C., Cao, A., Zeng, G., Liu, Z.: Dreamgaussian4d: Generative 4d gaussian splatting. arXiv preprint (2023) [9](#)
34. Seo, J., Jang, W., Kwak, M.S., Ko, J., Kim, H., Kim, J., Kim, J.H., Lee, J., Kim, S.: Let 2d diffusion model know 3d-consistency for robust text-to-3d generation. In: ICLR (2024) [3](#)

35. Shao, R., Zheng, Z., Tu, H., Liu, B., Zhang, H., Liu, Y.: Tensor4d: Efficient neural 4d decomposition for high-fidelity dynamic reconstruction and rendering. In: CVPR (2023) 3
36. Shi, Y., Wang, P., Ye, J., Long, M., Li, K., Yang, X.: Mvdream: Multi-view diffusion for 3d generation. arXiv preprint (2023) 3
37. Singer, U., Polyak, A., Hayes, T., Yin, X., An, J., Zhang, S., Hu, Q., Yang, H., Ashual, O., Gafni, O., et al.: Make-a-video: Text-to-video generation without text-video data. In: ICLR (2023) 5
38. Singer, U., Sheynin, S., Polyak, A., Ashual, O., Makarov, I., Kokkinos, F., Goyal, N., Vedaldi, A., Parikh, D., Johnson, J., et al.: Text-to-4d dynamic scene generation. In: ICML (2023) 2, 4
39. Tang, J., Ren, J., Zhou, H., Liu, Z., Zeng, G.: Dreamgaussian: Generative gaussian splatting for efficient 3d content creation. In: ICLR (2024) 9
40. Tang, J., Wang, T., Zhang, B., Zhang, T., Yi, R., Ma, L., Chen, D.: Make-it-3d: High-fidelity 3d creation from a single image with diffusion prior. In: ICCV (2023) 3
41. Tsalicoglou, C., Manhardt, F., Tonioni, A., Niemeyer, M., Tombari, F.: Textmesh: Generation of realistic 3d meshes from text prompts. In: 3DV (2024) 3
42. Wang, P., Liu, L., Liu, Y., Theobalt, C., Komura, T., Wang, W.: Neus: Learning neural implicit surfaces by volume rendering for multi-view reconstruction. In: NeurIPS (2021) 1
43. Wang, Z., Lu, C., Wang, Y., Bao, F., Li, C., Su, H., Zhu, J.: Prolificdreamer: High-fidelity and diverse text-to-3d generation with variational score distillation. In: NeurIPS (2023) 1, 3
44. Wang, Z., Bovik, A.C., Sheikh, H.R., Simoncelli, E.P.: Image quality assessment: from error visibility to structural similarity. IEEE TIP (2004) 8
45. Woo, S., Park, B., Go, H., Kim, J.Y., Kim, C.: Harmonyview: Harmonizing consistency and diversity in one-image-to-3d. In: CVPR (2024) 9
46. Wu, G., Yi, T., Fang, J., Xie, L., Zhang, X., Wei, W., Liu, W., Tian, Q., Xinggang, W.: 4d gaussian splatting for real-time dynamic scene rendering. In: CVPR (2024) 3
47. Wu, J., Gao, X., Liu, X., Shen, Z., Zhao, C., Feng, H., Liu, J., Ding, E.: Hd-fusion: Detailed text-to-3d generation leveraging multiple noise estimation. In: WACV (2024) 3
48. Xu, D., Jiang, Y., Wang, P., Fan, Z., Wang, Y., Wang, Z.: Neurallift-360: Lifting an in-the-wild 2d photo to a 3d object with 360deg views. In: CVPR (2023) 3
49. Yang, Z., Gao, X., Zhou, W., Jiao, S., Zhang, Y., Jin, X.: Deformable 3d gaussians for high-fidelity monocular dynamic scene reconstruction. In: CVPR (2024) 3
50. Yin, Y., Xu, D., Wang, Z., Zhao, Y., Wei, Y.: 4dgen: Grounded 4d content generation with spatial-temporal consistency. arXiv preprint (2023) 9
51. Zhang, R., Isola, P., Efros, A.A., Shechtman, E., Wang, O.: The unreasonable effectiveness of deep features as a perceptual metric. In: CVPR (2018) 9
52. Zhu, J., Zhuang, P.: Hifa: High-fidelity text-to-3d with advanced diffusion guidance. In: ICLR (2024) 3
53. Zitnick, C.L., Kang, S.B., Uyttendaele, M., Winder, S., Szeliski, R.: High-quality video view interpolation using a layered representation. In: ACM TOG (2004) 3
54. Zwicker, Pfister, Baar, V., Gross: Ewa volume splatting. In: Visualization, Vis (2001) 8